Neuro-Oncology Advances
4(1), 1–12, 2022 | https://doi.org/10.1093/noajnl/vdac117 | Advance Access date 21 July 2022

An affinity for brainstem microglia in pediatric high-grade gliomas of brainstem origin

Liat Peretz Zats, Labiba Ahmad, Natania Casden, Meelim J. Lee, Vitali Belzer, Orit Adato, Shaked Bar Cohen, Seung-Hyun B. Ko, Mariella G. Filbin, Ron Unger, Douglas A. Lauffenburger, Rosalind A. Segal, and Oded Behar

Department of Developmental Biology and Cancer Research, Faculty of Medicine, The Institute for Medical Research Israel-Canada, The Hebrew University, Jerusalem, Israel (L.P.Z., L.A., N.C., V.B., S.B.C., O.B.); Department of Biological Engineering, Massachusetts Institute of Technology, Cambridge, MA (M.J.L., S.-H.B.K., D.A.L.); Faculty of Life Sciences, Bar Ilan University, Ramat Gan, Israel (O.A., R.U.); Department of Pediatric Oncology, Dana-Farber Boston Children's Cancer and Blood Disorders Center, Boston, MA (M.G.F.); Department of Neurobiology, Harvard Medical School, Boston, MA, USA; Departments of Cancer Biology and Pediatric Oncology, Dana-Farber Cancer Institute, Boston, MA (R.A.S.)

Corresponding Author: Oded Behar, PhD, Department of Developmental Biology and Cancer Research, Faculty of Medicine, The Institute for Medical Research Israel-Canada, The Hebrew University, Ein Kerem, P.O. Box 12271, Jerusalem 91120, Israel (oded.behar@mail.huji.ac.il)

Abstract

Background. High-grade gliomas (HGG) in children have a devastating prognosis and occur in a remarkable spatiotemporal pattern. Diffuse midline gliomas (DMG), including diffuse intrinsic pontine gliomas (DIPG), typically occur in mid-childhood, while cortical HGGs are more frequent in older children and adults. The mechanisms behind this pattern are not clear.

Methods. We used mouse organotypic slice cultures and glial cell cultures to test the impact of the microenvironment on human DIPG cells. Comparing the expression between brainstem and cortical microglia identified differentially expressed secreted proteins. The impact of some of these proteins on DIPGs was tested.

Results. DIPGs, pediatric HGGs of brainstem origin, survive and divide more in organotypic slice cultures originating in the brainstem as compared to the cortex. Moreover, brainstem microglia are better able to support tumors of brainstem origin. A comparison between the two microglial populations revealed differentially expressed genes. One such gene, interleukin-33 (IL33), is highly expressed in the pons of young mice and its DIPG receptor is upregulated in this context. Consistent with this observation, the expression levels of IL33 and its receptor, IL1RL1, are higher in DIPG biopsies compared to low-grade cortical gliomas. Furthermore, IL33 can enhance proliferation and clonability of HGGs of brainstem origin, while blocking IL33 in brainstem organotypic slice cultures reduced the proliferation of these tumor cells.

Conclusions. Crosstalk between DIPGs and the brainstem microenvironment, in particular microglia, through IL33 and other secreted factors, modulates spatiotemporal patterning of this HGG and could prove to be an important future therapeutic target.

Key Points

- Diffuse intrinsic pontine gliomas (DIPGs) divide more in the brainstem environment compared to the cortex.
- Interleukin-33 (IL33) expression in brainstem and brainstem microglia is higher than in the cortex of young mice.
- IL33 propagates DIPG tumorigenesis, and its inhibition decreases DIPG proliferation.

© The Author(s) 2022. Published by Oxford University Press, the Society for Neuro-Oncology and the European Association of Neuro-Oncology.
This is an Open Access article distributed under the terms of the Creative Commons Attribution License (https://creativecommons.org/licenses/by/4.0/), which permits unrestricted reuse, distribution, and reproduction in any medium, provided the original work is properly cited.

Importance of the Study

Pediatric gliomas can arise in the supratentorial cerebral cortex with a median diagnosis age of 13 years, while diffuse midline gliomas (DMGs), present a median diagnosis age of 7 years, and appear most frequently in the pons. DMGs have a devastating prognosis and are currently untreatable. We tested the contribution of the brainstem microenvironment to the observed spatiotemporal pattern of pediatric high-grade gliomas. Our results support a model in which the brainstem microenvironment, particularly microglia, offers more supportive conditions for diffuse intrinsic pontine gliomas (DIPG) cells. By using the differences in gene expression between brainstem and cortical microglia, we were able to identify factors that may contribute to the DIPG preference toward the brainstem. In this study, we focused on the factor interleukin-33 and provided evidence to support its contribution to the propagation of DIPGs in this specific anatomical location.

High-grade gliomas (HGGs) constitute 8%–10% of brain tumors in children and usually cause death within 2 years of diagnosis.[1] Pediatric gliomas can arise in the supratentorial cerebral cortex or in infratentorial regions, such as the cerebellum, brainstem, midbrain, thalamus, and spine.[2] Approximately half of pediatric high-grade gliomas (pHGGs) arise in midline locations, specifically in the thalamus and the pons, and are classified as diffuse midline gliomas (DMGs; pontine DMG is also known as diffuse intrinsic pontine glioma [DIPG]). While pontine and thalamic DMGs typically occur in mid-childhood, pediatric cortical gliomas occur in older children and young adults, and HGGs of later adulthood occur mainly in the frontotemporal lobes.[2]

Recent studies make it increasingly apparent that supratentorial and infratentorial pHGGs differ from one another and from their adult counterparts. In particular, the predominant oncogenic mutations vary depending on location and on the patient's age. A striking example is the lysine to methionine mutation on residue 27 in histones H3.1 (H3.1K27M) and H3.3 (H3.3K27M) observed in approximately 80% of pontine DMG cases in younger children, while tumors with H3.3G34R/V mutations usually occur in the cerebral hemispheres of adolescents and young adults.[2–4]

One possible explanation for this remarkable spatiotemporal pattern of DMGs may be a local advantage of the microenvironment of the infratentorial regions in a restricted time frame that fosters the development of tumors carrying these specific mutations. This assumption is consistent with the limited ability to induce tumorigenic transformations in older mice when using genes associated with DIPG mutations.[5]

A preference for pontine DMGs toward the young brainstem would imply that specific cells at a restricted time point in this location may be more suitable for the formation, progression and survival of such tumors. If specific cell types in the brainstem indeed give an advantage to the formation of DIPG tumors, such cells should have differential anatomical and developmental properties. Consistent with this idea, accumulating evidence indicates that various cells in the CNS such as astrocytes, oligodendrocytes, and microglia show some anatomical and functional differences.[6–10]

Evidence for interaction and crosstalk between microglia, astrocytes, and vascular cells in adult forms of glioma has been previously demonstrated.[11–13] Pediatric brain tumors were also recently shown to be influenced by their environment.[14,15] In this case, activated neurons in the microenvironment were shown to promote glioma growth.

In this work, we tested the possibility that pontine DMGs of brainstem origin are more attuned to brainstem surroundings, and subsequently aimed to find an anatomically specific DIPG–microenvironment crosstalk contributing to this compatibility.

Materials and Methods

Animals: C57BL/6 mice were obtained from ENVIGO (Rehovot, Israel). Animal handling adhered strictly to national and institutional guidelines for animal research and was approved by the Ethics Committee of the Hebrew University. Mice both males and females between days 2 and 4 after birth were used.

Antibodies: a list of antibodies is in Supplementary methods.

Immunostaining and Western blot: explanation is found in Supplementary methods.

Patient-derived tumor cell cultures

All cultures were maintained as neurospheres in tumor stem medium (TSM) consisting of 50% Neurobasal(-A)/50% DMEM/F12, supplemented with B27™(-VitA) and growth factors as described previously[14] and in Supplementary methods.

GFP + or luciferase DIPG cell line preparation.—Each patient-derived HGG cell line was infected with Lenti-GFP/Luciferase viral supernatant and allowed to recover for 1 week. GFP-positive cells were isolated for purity by fluorescence-activated single cell sorting (FACS) (BD FACS Aria) and returned to culture. Luciferase-positive cells were isolated via Puromycin (1 μg/ml) selection. Validation of the sorting was done using flow cytometry analysis and by observing the cell fluorescence under the microscope (with at least a 90% positive GFP rate).

Slice culture preparations.—Tumor cells (10,000 cells/μl) were re-suspended in Matrigel (Corning, NY, USA) and TSM (1:1) and injected (1 μl) using Narishige MM-3

micromanipulator (Tokyo, Japan). The cells were systematically injected in parallel into both the brainstem and cortex of P2–4 mouse brains, two injections per region. The injections of each region were performed consecutively, alternating the order of injections between brainstem and cortex. After injections, the brain regions were gently separated and tissue pieces were incubated on top of 40-µm cell filters. Each well was filled with medium (Neurobasal, 15 mg/ml glucose, AmphoB 25 µg/ml, Pen-Strep, and B27 [without vitA]) up to the level of the filter to allow diffusion. Incubation was for 24–72 h in 5% CO_2, 37° C.

Ex vivo multiphoton imaging and quantification

Each injected cortex and brainstem pair was incubated for 24 h, then sealed with a cover slip (moisturized with phosphate-buffered saline (PBS)) and imaged live, using the large image option of *Nis-Elements*, and the maximal width in the Z stack option so as to capture all of the injected GFP + cells. The analysis is described in Supplementary methods.

Ex vivo GFP quantification analysis.—After 24 h, slices were dissociated and analyzed in a Fortessa LSR cell analyzer (BD Biosciences, CA, USA). We made sure to record all of the events from each sample (about 3–8 million events per sample), so that quantification represents the absolute GFP + cell count per brain region injected. For each cell line, at least 9 brains were injected, in at least 3 injection sessions.

Ex vivo CellTrace proliferation analysis.—Glioma cells were labeled with CellTrace reagent and injected into mouse brains as previously described (CellTrace™ Violet Cell Proliferation Kit, for flow cytometry, Thermofisher, MA, USA). A T0 measurement (maximal CellTrace intensity) was obtained per trial and used to determine the percentage of dividing cells after 24- or 72-h incubation.

Ex vivo cell death analysis.—Following slice culture incubation of either 6 or 24 h, injected tissue samples were dissociated and stained with 100 µg/ml Propidium Iodide (PI) (Thermofisher, MA, USA). Flow cytometry was used to quantify the percentage of PI-positive cells out of GFP-positive cells.

Microglia and astrocytes cell culture

Preparation of mixed glia primary cell cultures and astrocytes from 2- to 3-day-old mice was previously described.[16] Microglia were prepared as described here.[17] Briefly, to produce an astrocyte cell culture, the cells are plated in very low density, 20 ng/ml EGF (PeproTech, Rehovot, Israel) is applied in the first few days, and when confluent the culture gets shaken overnight, treated with AraC (0.1 mM, Sigma Aldrich) and passaged twice in order to ensure purity. For microglia isolation, mixed glial cells were plated densely and treated with 0.5 ng/ml gmCSF (PeproTech, Rehovot, Israel), until the cells are easily isolated from the culture and plated for experiments. An extended explanation is found in Supplementary methods.

qPCR DNA quantification.—Testing of cell number with DNA-based qPCR and primers was carried out based on a previous paper with some modifications.[18] Briefly, DNA from a controlled number of glioma and mouse (astrocytes and microglia) cells was acquired, then a qPCR reaction (iTaq Universal SYBR Green Supermix, BioRad, Rishon Le Zion, Israel) using either a human-specific primer or a primer designed to detect both human and mouse cells was performed on the control DNA samples. (Oligonucleotide sequences can be found in Supplementary methods.) The results were used to create transformation formulas from cycle threshold (CT) to cell number/DNA amount with a high prediction power ($R^2 = 0.99$ for both primers). To test the strength of these transformation formulas, sets of quantified human and mouse DNA samples (from 100% human DNA, 90% human with 10% mouse, etc., all the way to 100% mouse DNA) were tested. Using our transformation formula, we were able to accurately estimate the ratio of mouse and human cells in a mixed culture, with a strong predictive value ($R^2 = 0.98$).

Co-culture proliferation experiments.—Eight thoushand human HGGs were placed on top of mouse glial cell cultures (12 well)—astrocytes and microglia, originating either in the brainstem or the cortex of the same mice. For each condition, within each trial, T0 wells were acquired about 2 h after the trial began. The co-culture was then incubated for 72 h in glioma medium, after which DNA was acquired using the Monarch DNA cleanup kit (NEB, Ipswich, MA, USA), and DNA-based qPCR quantification was done, as described above.

Microglial conditioned medium preparation. For each trial, a confluent microglial cell culture was prepared, taking care to maintain similar conditions for the brainstem and cortical derived microglia. Once cell cultures reached a similar confluence, the cells were thoroughly washed to remove any residual serum, and TSM without factors was added. For each 4-cm^2 well, 1.5 ml of medium was added. After 72 h, the medium was collected and filtered.

Luciferase-based viability assay. Luciferase-labeled DIPG cells were plated on top of purified microglia or astrocytes (670 cells/well), in 0.3-cm^2 wells. Following a 72-h incubation, luciferase activity was measured using LUMIstar® Omega (BMG LABTECH, Ortenberg, Germany) microplate luminescence reader. Each experiment consisted of a minimum of 4 wells per condition, and each experiment was repeated at least 6 times per cell line.

Three-dimensional growth experiments. Recombinant human IL33 (50 ng/ml, PeproTech, Rehovot, Israel) was added to a TSM and Matrigel mixture (1:1 ratio) with DIPG cells highly concentrated to create very dense cell-matrigel droplets. These marked a specific starting point. Control droplets were also added. After the initial solidifying of the gel, the radius of the droplet was expanded by adding more Matrigel–TSM mix. After final solidification, TSM-based

medium was added on top of the Matrigel drops to cover them. The diameter of each DIPG drop was measured after 2 h and 7 days. ImageJ was used to measure the change in diameter. In each trial, at least 7 droplets for each condition were used.

Proliferation experiments. CellTiter-Glo® Luminescent Cell Viability Assay (Promega, Madison, WI, USA) was used as described in Supplementary methods in the "Recombinant IL33 concentration calibration."

Colony count and average colony size experiments. Four hundred DIPG cells were plated in 0.3-cm^2 wells. This low-density plating allowed clear segregation of colonies. For each condition, at least 7 wells were plated per repeat. After 5 days incubation, the cultures were analyzed using Incucyte® S3 (Sartorius, Göttingen, Germany) Live-Cell Analysis system (whole well image X4).

RNA-sequencing analysis.—RNA data processing, data analysis, and subcellular localization analysis are described in Supplementary methods.

PedcBiPortal gene expression.—Data and the clinical data associated with each sample were downloaded from the PedcBioPortal (https://pedcbioportal.kidsfirstdrc.org/)[19,20] on February 2022. Data analysis is described in Supplementary section.

mIL33 neutralization trial in ex vivo slice cultures

DIPG cells, labeled with CellTrace Dye, were injected with 1 μg/ml of mIL33 antibody or isotype control antibody into each side of the cortex and of the brainstem, then slice cultures were prepared. After 3 days, the proliferation of DIPGs within each condition was measured using flow cytometry analysis. An additional cortical injection was used to exclude any brains in which no brainstem preference was detected from the statistical analysis, excluded brains: DIPGXIII 3/13, DIPGXXV 1/12, BT869 3/14.

shRNA IL1RL1 knockdown.—This was performed essentially as previously described.[21] For IL1RL1 knockdown experiments, we used Mission® shRNA PLKO lentiviral vectors which include puromycin selection marker: TRCN0000358832/sh-IL1R-1 and TRCN0000058513/sh-IL1R-2. For a control, we used an empty vector (pLKO.1-puro); all vectors purchased from Sigma Aldrich (St. Louis, MO, USA). Details are described in Supplementary section.

qPCR Analysis.—This was performed essentially as previously described.[21] Differential expression was determined using the delta CT method. Each primer set was tested on human and mouse samples to make sure each primer is species specific. Further details are in Supplementary methods.

Statistical analysis.—Generally, non-parametric, coupled (Wilcoxon) or un-coupled (Mann–Whitney), one-tailed statistical tests were applied. Details are described in Supplementary methods.

Results

Preference of pediatric HGGs of brainstem origin toward the brainstem

To test the intrinsic compatibility of DIPGs to their anatomical origin, we adopted an ex vivo approach, which allowed us to test the initial response of DIPGs to their microenvironment. We injected equal numbers of GFP-labeled, patient-derived DIPG cells into the brainstem and cortex of the same brains followed by organotypic slice cultures. Using two-photon microscopy (Figure 1a–c), we detected higher numbers and a broader distribution of DIPG cells in the brainstem slices in comparison to the cortex.

To quantify the number of tumor cells in each region, we used flow cytometry analysis. In all DIPGs tested, more cells were present in the brainstem. In contrast, the pediatric HGG of cortical origin, KNS-42, showed a strong preference toward the cortex, while another cortical line, SU-pcGBM2, showed no preference to either site (Figures 1d and S1).

To test proliferation, we used CellTrace™ dye at 24 and 72 h (Figure 1e). At 24 h, there was very little DIPG division overall, suggesting improved survival as opposed to proliferation in the brainstem at this time point. To test this directly, tumor cell death in the slice cultures was analyzed. After 6 h (Figure 1f), cells from all DIPG lines died less in the brainstem while SU-pcGBM2 showed an opposite response. At 24 h (Figure S2), only BT869 and pcGBM maintained their original preference while the other lines showed no significant difference (Figure S2). Surprisingly, KNS-42 died less in the brainstem. We then tested proliferation after 72 h, when initial difference in proliferation was detected. We found significantly more DIPG division in the brainstem. In contrast, SU-pCGBM2 and KNS-42 showed a trend toward the cortex although this was not statistically significant (Figures 1g and S3).

Brainstem microglia increase the accumulation of HGGs of brainstem origin

To assess the glial cells' contribution, we tested the proliferation of SU-DIPGXIII on mixed glial cultures from the brainstem and cortex using a DNA-based qPCR approach. We calculated the estimated proportion of DIPG cells according to cycle threshold, based on calibration curves prepared with known numbers of human and mouse cell mixes (Figure S4). Interestingly, DIPG cells proliferated significantly more when incubated with brainstem glia (Figure 2a). Since microglia are known to infiltrate the tumor microenvironment and contribute considerably to glioma development,[22–25] we decided to test their role. DIPGs were plated with purified microglia from each brain region. Tumor cell number was estimated using the DNA-based qPCR quantification described above. All HGGs of brainstem origin accumulated significantly more on brainstem microglia, while SU-pCGBM2 did not (Figures 2b and S5a). In contrast, DIPGs showed no anatomical preference

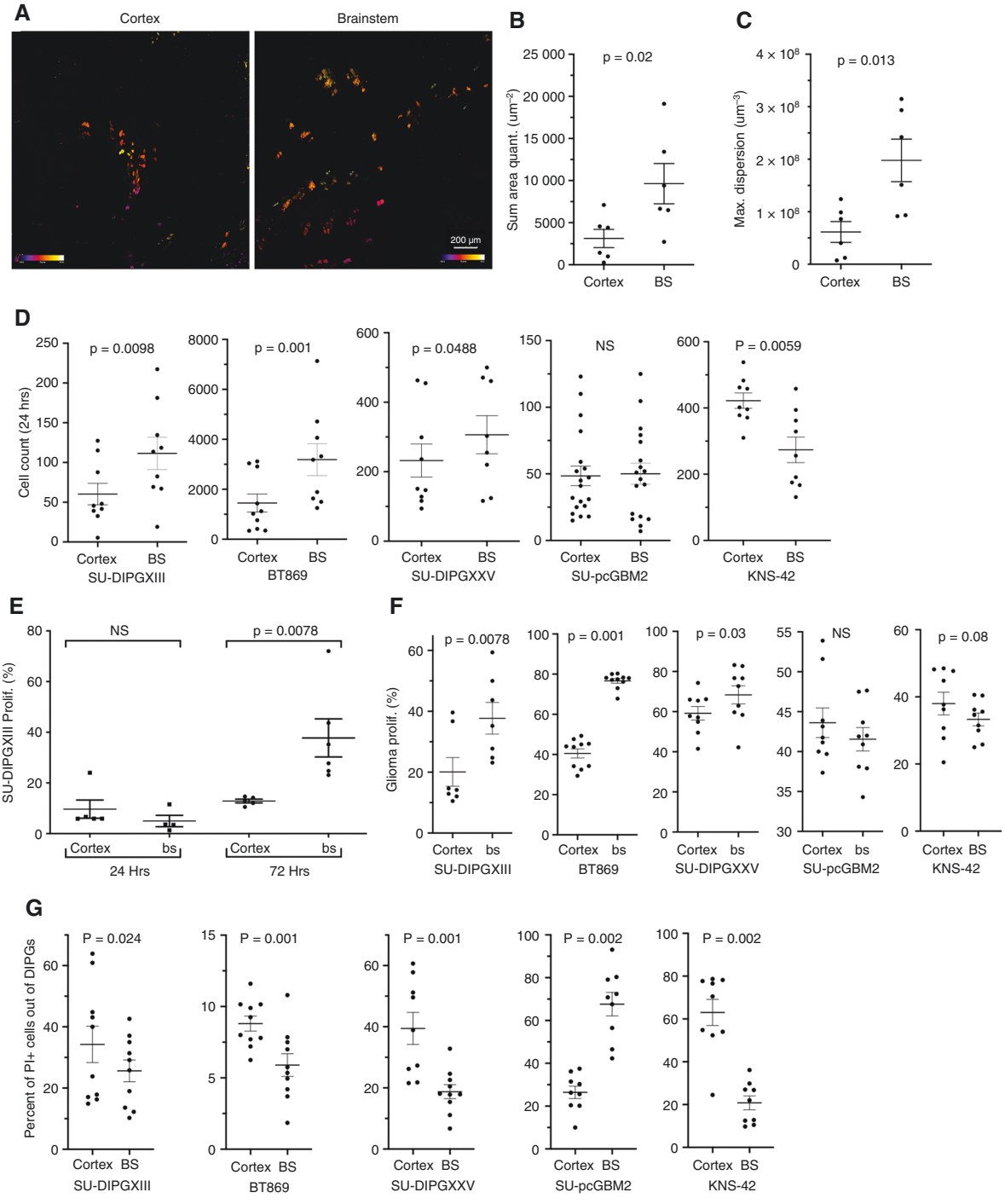

Figure 1. Preference of pediatric HGGs of brain stem origin toward the brainstem. (a) Two-photon micrograph of infiltrating SU-DIPGXIII cells expressing eGFP, 24-h postinjection into P2 mouse brain. (b) Nis-elements analysis of eGFP-positive cell amount in each micrograph (Mann–Whitney *U* test; $n = 6$). (c) Diffusion quantification of eGFP-positive cells within each micrograph measuring the 3-dimensional maximal area (um^3) (Mann–Whitney *U* test; $n = 6$). (d) Flow cytometry analysis was used to quantify the total glioma count in each sample, 24-h postinjection ± SEM (Wilcoxon's signed-rank test, one-tailed; SU-DIPGXIII $n = 9$, BT869 $n = 10$, SU-DIPGXXV $n = 9$, SU-pcGBM2 $n = 9$, KNS-42 $n = 9$). (e) Flow cytometry analysis of CellTrace dye staining of GFP + SU-DIPGXIII cells. Data presented as the average percent of proliferation of glioma population ± SEM (Wilcoxon's signed-rank test, one-tailed; $n = 6$-7). (f) Flow cytometry analysis of PI staining of GFP + glioma cells 6-h postinjection into the cortex and brainstem of the same brain. Each point represents the percentage of PI + cells out of the GFP + population, indicating glioma cell death ± SEM. (Wilcoxon's signed-rank test, one-tailed; -DIPGXIII $n = 10$,BT869 $n = 10$, SU-DIPGXXV $n = 10$, SU-pcGBM2 $n = 9$, KNS-42 $n = 9$). (g) Flow cytometry analysis of CellTrace dye staining of GFP + glioma cells 72-h postinjection into the cortex and brainstem of the same brain. Each point on the graph represents the percentage of GFP + cells which underwent division (at least 1), out of the entire GFP + cell population ± SEM (Wilcoxon's signed-rank test, one-tailed; -DIPGXIII $n = 7$, BT869 $n = 10$, SU-DIPGXXV $n = 9$, SU-pcGBM2 n = 11, KNS-42 $n = 9$).

on astrocytes (Figures 2c and S5b), while SU-pcGBM2 proliferated more on cortical astrocytes. Although microglia and astrocytes are altered and activated in culture, we assumed these alterations occur in cells from both regions, allowing an informative comparison.

To validate the DNA qPCR results, two DIPG lines labeled with luciferase were used to estimate DIPG accumulation on microglia or astrocytes, with similar results (Figures 2d,e and S5c). As a final validation step for the effects of microglial cells on DIPGs, we used anti-human-specific

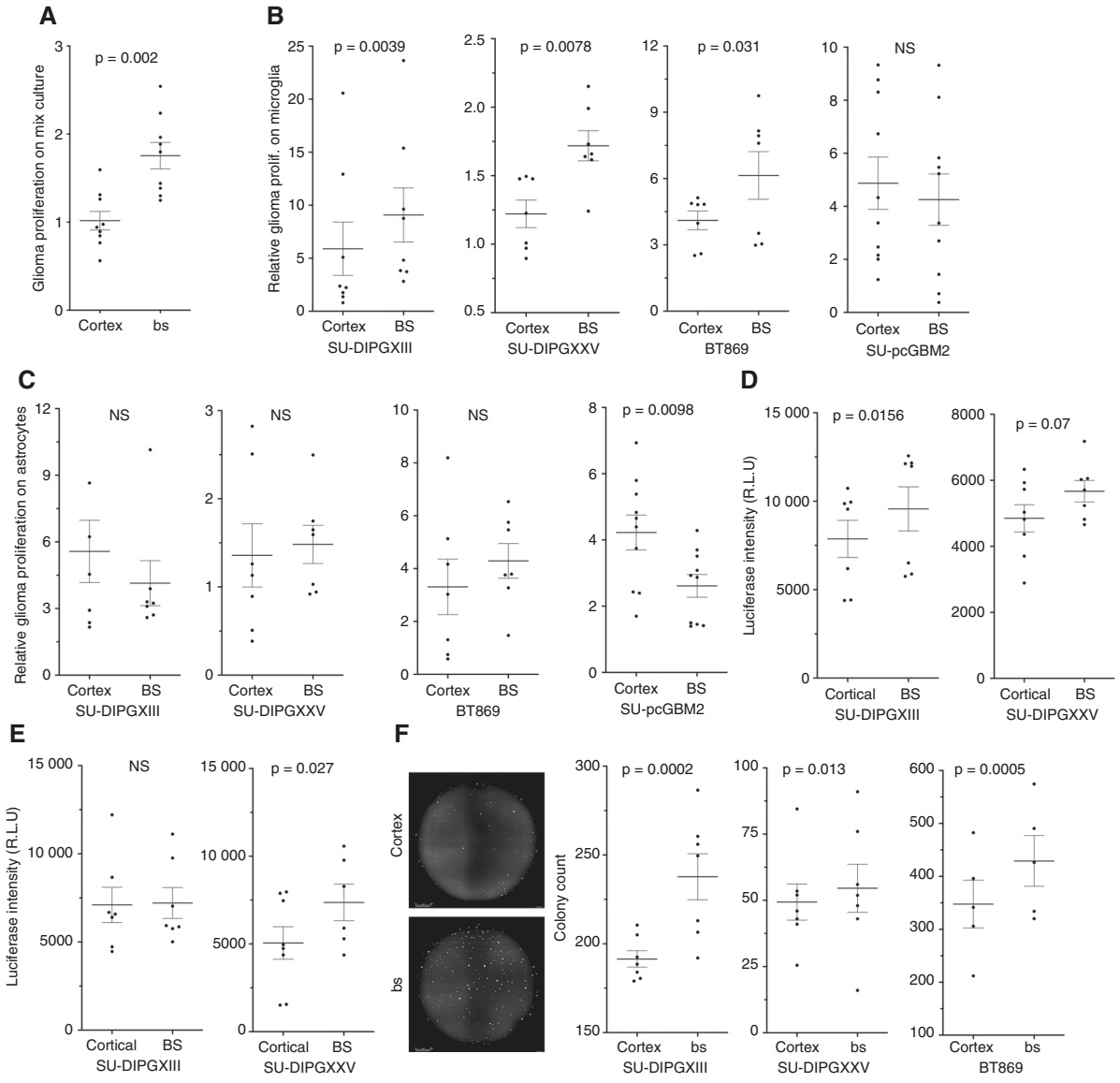

Figure 2. Microglia are responsible for brainstem differential effect on brainstem-derived glioma cell lines (DIPGs). (a) Glioma cell quantification using qPCR on human genomic DNA; DNA acquired from co-cultures of mouse-mixed glia and human SU-DIPGXIII. The data are presented as the average fold change per trial, after 72 h compared to $T = 0 \pm$ SEM. Each point on the graph represents the average of at least 4 repeats. (Wilcoxon's signed-rank test; $n = 9$. One tailed). (b, c) Glioma cell co-culture proliferation. The proportion of the tumor within the co-culture was estimated using qPCR on human/mouse genomic DNA; the DNA was acquired from mouse microglia (b) or astrocytes (c) and human glioma co-cultures after 3 days of incubation. The data are presented as the average fold change per trial after 72 h, compared to $T = 0 \pm$ SEM (each point on the graph represents an average of at least 3 repeats) (Wilcoxon's signed-rank test, one-tailed; SU-DIPGXIII $n = 8$, SU-DIPGXXV $n = 7$, BT869 $n = 7$, SU-pcGBM2 $n = 11$). (d, e) DIPG co-culture proliferation quantified with a luciferase-based assay. Luciferase-positive DIPG lines were incubated on top of brainstem or cortical derived microglia (d) or astrocytes (e). After 72 h, the luciferase intensity was quantified, and the data are presented in Relative Luminescence Units (each point on the graph represents the average of at least 3 repeats). (Wilcoxon's signed-rank test, one-tailed; SU-DIPGXIII $n = 8$, SU-DIPGXXV $n = 8$). (f) The effect of microglial-derived conditioned medium on clonability properties of DIPG cultures (representative image—left). The colony count per well is presented as ± SEM; each point represents a median count of 8 repeats (Fisher's Combined Probability Test; SU-DIPGXIII $n = 7$, SU-DIPGXXV $n = 5$, BT869 $n = 7$. Within each trial, a Mann–Whitney U test was performed to obtain the p-values. One tailed).

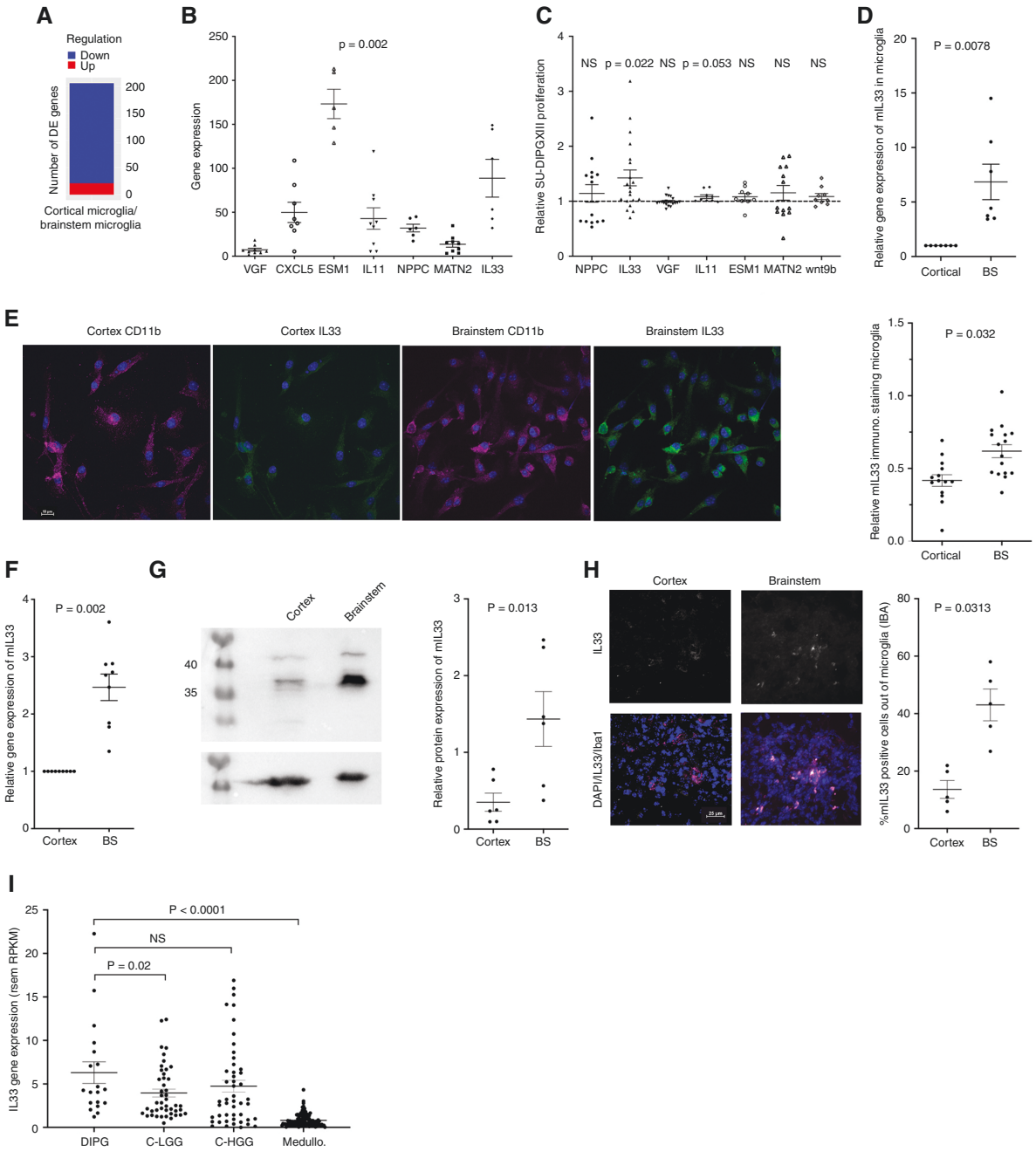

Figure 3. Differential gene expression between brainstem and cortical microglia. (a) Global gene analysis of brainstem and cortical microglia using RNA-seq approach. Chart summarizing number of DEGs, where DEGs are genes that had abs{log2FoldChange} > 1 and padj < 0.05, after DESeq2analysis. Regulation was determined by the sign of log2FoldChange, wherelog2FoldChange > 0 indicated upregulation while log2FoldChange < 0 indicated downregulation in the first sample of each comparison. The comparison shown refers to gene expression change of cortical microglia on SU-DIPGXIII against brainstem microglia on SU-DIPGXIII. There are 21 upregulated and 185 downregulated genes in this comparison ($n = 3$ from each sample analyzed). (b) Quantitative PCR analysis was done on at least 6 separate SU-DIPGXIII + microglia co-culture trials, per gene tested. The values are expressed as the average fold change in brainstem co-cultures in comparison to the corresponding cortical co-cultures, ± SEM. (Wilcoxon's signed-rank test; NPPC and IL33 $n = 6$; MATN2, VGF, IL11, and ESM1 $n = 9$, wnt9b $n = 8$. One tailed). (c) Screening of selected secreted factors, isolated from RNA-seq analysis, for positive proliferation effects on SU-DIPGXIII. Glioma cells were incubated with control medium or with a factor for 72 h, after which proliferation was measured using the CellTiter-Glo luminescence system. The data are presented as the average fold change of the secreted factor's effect as compared to the control ± SEM. (Wilcoxon's signed-rank test; NPPC, MATN2 $n = 14$, IL33, VGF $n = 20$, Epha3, Wnt9b, IL11, ESM1 $n = 9$. One-tailed, Bonferroni correction for multiple comparisons was applied). (d) Quantitative PCR analysis of mouse IL33 gene expression in pure microglial cell cultures. The values are expressed as the average fold change in brainstem cultures in comparison to the corresponding cortical cultures ± SEM. (Wilcoxon's signed-rank test; $n = 7$). (e) Representative immunofluorescence for IL33 and CD11b on brainstem or cortical microglia (scale bar 10 μm). Analysis was performed with Nis-elements by measuring the ratio of

antibody to identify and count SU-DIPGXIII cells with a comparable outcome (Figure S6). Altogether, a clear intrinsic preference of DIPGs to brainstem microglia was documented.

To test the involvement of secreted factors, a conditioned medium from brainstem and cortical microglial cell cultures (incubated without tumor cells) was used in a colony formation assay. In all DIPGs tested, the number of colonies was significantly higher with brainstem conditioned media (Figure 2f). Thus, at least part of the propagative influence of brainstem microglia is mediated by secreted factors.

Differential gene expression between brainstem and cortical microglia

Based on the observed functional difference between microglia of brainstem and cortical origin, we analyzed the differences in gene expression between them. Since HGGs and microglial cells might impact each other's gene expression, microglia were incubated with SU-DIPGXIII. For gene expression analysis, the microglia–DIPGXIII sample data were aligned to a combined human and mouse reference genome. Though differences were detected, no statistically significant differences could be found in gene expression of the human genes (SU-DIPGXIII) by applying a uniform statistical cutoff. In contrast, mouse microglia revealed a significant number of differentially expressed genes (Figure 3a; Table S1).

To select relevant genes for analysis, we used the Uniprot database, and identified 92 protein-coding genes of secreted or membrane-associated proteins (Table S1). We then focused on potentially novel candidates with a high fold change and known links to cancer, particularly glioma. Based on these criteria, we selected 7 genes. To validate their differential expression, RNA from microglia-SU-DIPGXIII co-cultures was tested using mouse-specific qPCR analysis (Figure 3b).

Next, we tested the ability of proteins coded by these genes to induce the proliferation of SU-DIPGXIII (Figure 3c). Out of the 7 candidates, only IL33 significantly enhanced HGG proliferation. To test whether IL33's differential expression is intrinsic, we performed qPCR (Figure 3d) and immunostaining (Figure 3e) on purified microglia. Results indicated that this difference is indeed intrinsic. Consistent with this, the expression level of IL33 mRNA transcripts and protein is higher in the brainstem of mice at a young age (Figure 3f,g), with this higher expression being at least partly due to the expression in brainstem microglia (Figures 3h and S7). Furthermore, according to qPCR analysis, this anatomically differential expression significantly lessens at the age of 2 mo and is most significant from birth up to 8 weeks (Figure S8)

Interestingly, IL33 expression in DIPG patients is significantly higher than in patients with cortical low-grade glioma or medulloblastoma (Figure 3i). The higher expression levels of IL33 in human DIPGs and pediatric cortical HGG samples are consistent with the IL33 data in adult HGGs.[26–28] Since cellular resolution is lacking, the source of IL33 in DIPGs may be the microenvironment, as our data suggests, while in the cortical HGGs, the source could be the glioma cells, as has been shown for adult HGGs.[26,27]

IL33 is able to support DIPG tumor behavior in vitro and in slice cultures

To find the working concentration of IL33, we carried out a dose–response proliferation assay using DIPGXIII (Figure S9), and selected a concentration of 50 ng/ml, which is consistent with previous studies.[29–31] We then tested the effect of recombinant IL33 on DIPG proliferation (Figure 4a), 3D growth (Figures 4b and S10), and colony formation (Figures 4c and S11). In all DIPG lines tested, IL33 significantly enhanced tumorigenesis.

To test the role of IL33 in proliferation in the brainstem, we used CellTrace™-labeled DIPG cells injected into slice cultures, together with either IL33 blocking antibody or isotype control antibody (Figure 4d). All three DIPGs tested proliferated significantly less in the presence of the IL33 antibody (Figure 4d). The relatively modest effect might indicate limited accessibility of the antibody or perhaps the contribution of other factors present in the brainstem.

Expression of IL33 receptors in DIPGs

We explored the *PedcBioPortal* and found that expression levels of IL1RL1, IL33's binding receptor, are higher in DIPG and cortical HGG biopsies compared to expression levels in cortical low-grade cortical gliomas (Figure 5a), a result consistent with other studies in adult HGGs

Fig. 3 continued
mIL33-positive cells out of CD11b-positive cells. Quantification was done with the "sum area quantification" tool. (Fisher's Combined Probability Test; $n = 3$.Within each trial, a Mann–Whitney U test was performed to obtain the p-values, $n = 6$ fields. One tailed). (f) Quantitative PCR analysis of mouse IL33 gene expression in the brainstem and cortex of P2 mice. The values are expressed as the average fold change in the brainstems in comparison to the corresponding cortexes, ± SEM. (Wilcoxon's signed-rank test; $n = 9$). (g) A representative Western blot analysis of mIL33 expression in the brainstem and in the corresponding cortex of P2 mice. The graph shows a quantitative analysis of the Western blot trials, using GelQuant express, and then normalizing the mIL33 expression to the actin on the same membranes. At least 6 comparisons of brainstem-cortex were performed (Wilcoxon's signed-rank test; $n = 6$). (h) Representative immunofluorescence for IL33 (white) and Iba1 (magenta) on a brain slice, from either the brainstem or the cortex. (scale bar 25 μm). Analysis was performed with Nis-elements by measuring the percent of mIL33-positive cells out of Iba1-positive cells. Quantification was done with the "sum area quantification" tool. (Wilcoxon's signed-rank test; $n = 5$). (i) Human IL33 gene expression data obtained from PedcBioPortal. The gene's expression within biopsies from DIPG samples was compared to cortical low- and high-grade gliomas and to medulloblastoma biopsies. Each point on the graph represents a single human sample. FPKM = fragments per kilobase of exon per million mapped fragments, RSEM = RNA-Seq by Expectation-Maximization (Mann–Whitney U test was performed).

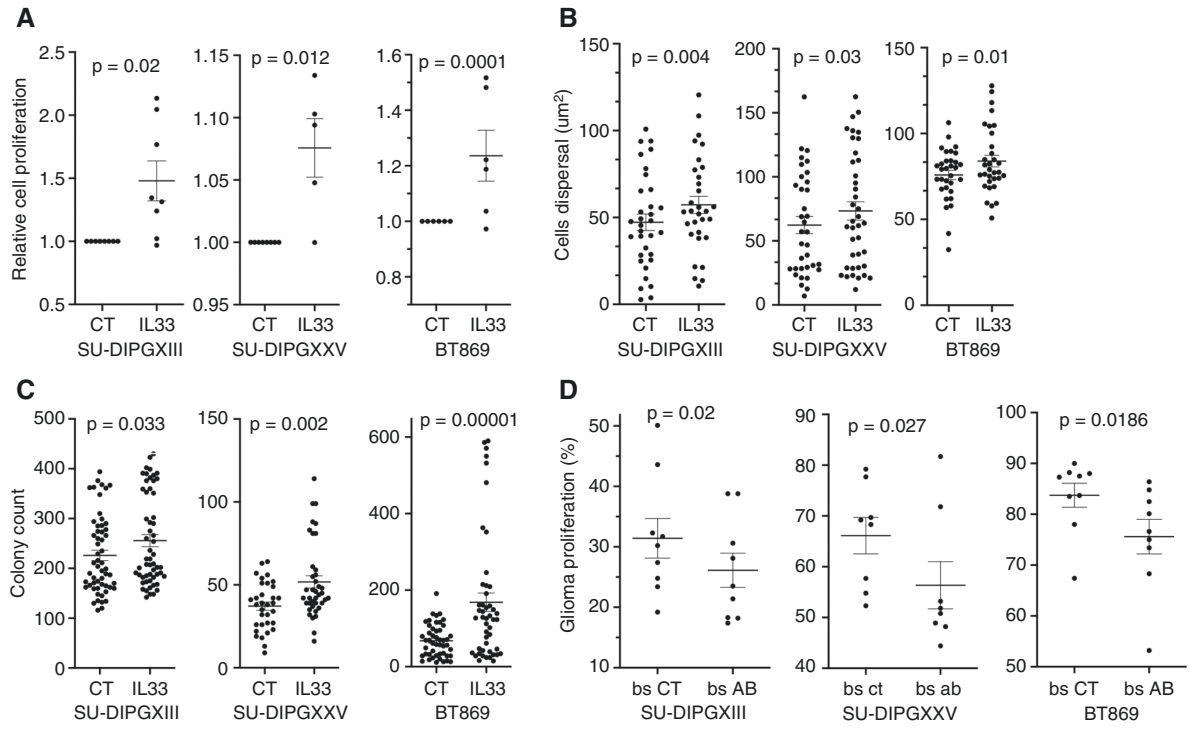

Figure 4. IL33 impacts DIPG proliferation, growth in 3D, and colony formation. (a) Proliferation of DIPG cells over a period of 72 h with IL33 (50 ng/ml) or control condition (CT). Proliferation was measured using CellTiter-Glo luminescence. The data are presented as the fold change in proliferation with IL33 treatment compared to control, each point represents the average of 8 repeats. (Wilcoxon's signed-rank test; SU-DIPGXIII $n = 8$, SU- DIPGXXV n = 6, BT869 n = 8). (b) Cells' dispersal diameter refers to the expansion of each DIPG line in a Matrigel—TSM mixture (1:1) with IL33 treatment, in comparison to the CT. The data were obtained by placing a concentrated droplet of DIPG cells in the center of each gel–TSM droplet and measuring the area of the DIPG droplet after 2 h (for a time zero measurement), and then comparing to the final area after 7 days. Images were obtained and the area measured, using ImageJ (Fisher's Combined Probability Test; SU-DIPGXIII $n = 6$, SU-DIPGXXV $n = 6$, BT869 $n = 5$. Within each trial, a Mann–Whitney U test was performed to obtain the p-values, $n = 7$ droplets. One tailed). (c) DIPG colony count per well, after a treatment period of 5–7 days with IL33 in comparison to control. Quantification was performed with Incucyte® S3 Live-Cell Analysis system (Fisher's Combined Probability Test; SU-DIPGXIII $n = 11$, SU-DIPGXXV $n = 8$, BT869 $n = 6$. Within each trial, a Mann–Whitney U test was performed to obtain the p-values, $n = 6$-8 wells. One tailed). (d) mIL33 neutralization trial in ex vivo slice cultures. Flow cytometry analysis of CellTrace dye staining of DIPG cells, injected with 1 μg/ml of mIL33 antibody or isotype control antibody. The cells were injected into two sides of the brainstem from a single P2 mouse brain, then slice cultures were prepared. After 72 h, the proliferation of DIPGs was measured (Wilcoxon's signed-rank test, one-tailed; SU-DIPGXIII $n = 10$, SU- DIPGXXV $n = 10$, BT869 $n = 11$, when n represents a single brain).

in which IL33 has been suggested to play a role.[26–28,31,32] Consistent with the biopsy data, IL1RL1 was expressed at much higher levels in SU-DIPGXIII cells injected into the brainstem (organotypic slice culture) as compared to cultured cells, while IL1-RAcP (IL33's co-receptor) was also affected, but more moderately (Figure 5b). Furthermore, both receptors were expressed at higher levels in cells injected into organotypic slice cultures of the brainstem in comparison to the cortex (Figure 5c,d), and on brainstem microglia (Figure 5e). To test the role of IL1RL1 signaling in DIPG proliferation, a knockdown approach was utilized. SU-DIPGXIII was treated with shRNAs targeting IL1RL1, and the effect was validated by qPCR (Figure S12). The knocked-down cells were then tested in an organotypic proliferation assay (Figure 5f). Consistent with the IL33 blocking experiments, targeting IL33's receptor reduced proliferation in the brainstem which as expected had no effect on proliferation in the cortex.

Discussion

In this study, we sought to begin exploring the mechanism underlying the observed spatiotemporal pattern of pediatric HGGs. Two explanations have been put forward in the past. One explanation suggests that the locations of pHGGs coincide with waves of myelination in the childhood and adolescent brains and so reflect tumor intrinsic factors, while a second possibility suggests that this pattern is due to the microenvironment. These two explanations are not necessarily mutually exclusive.

Here we tested the potential of the brainstem surroundings to differentially impact DIPGs' survival and proliferation. As compared to the cortex, the brainstem shows a potential to better support the progression of HGGs of brainstem origin. This was demonstrated by the increased survival and proliferation of DIPG tumors in the brainstem.

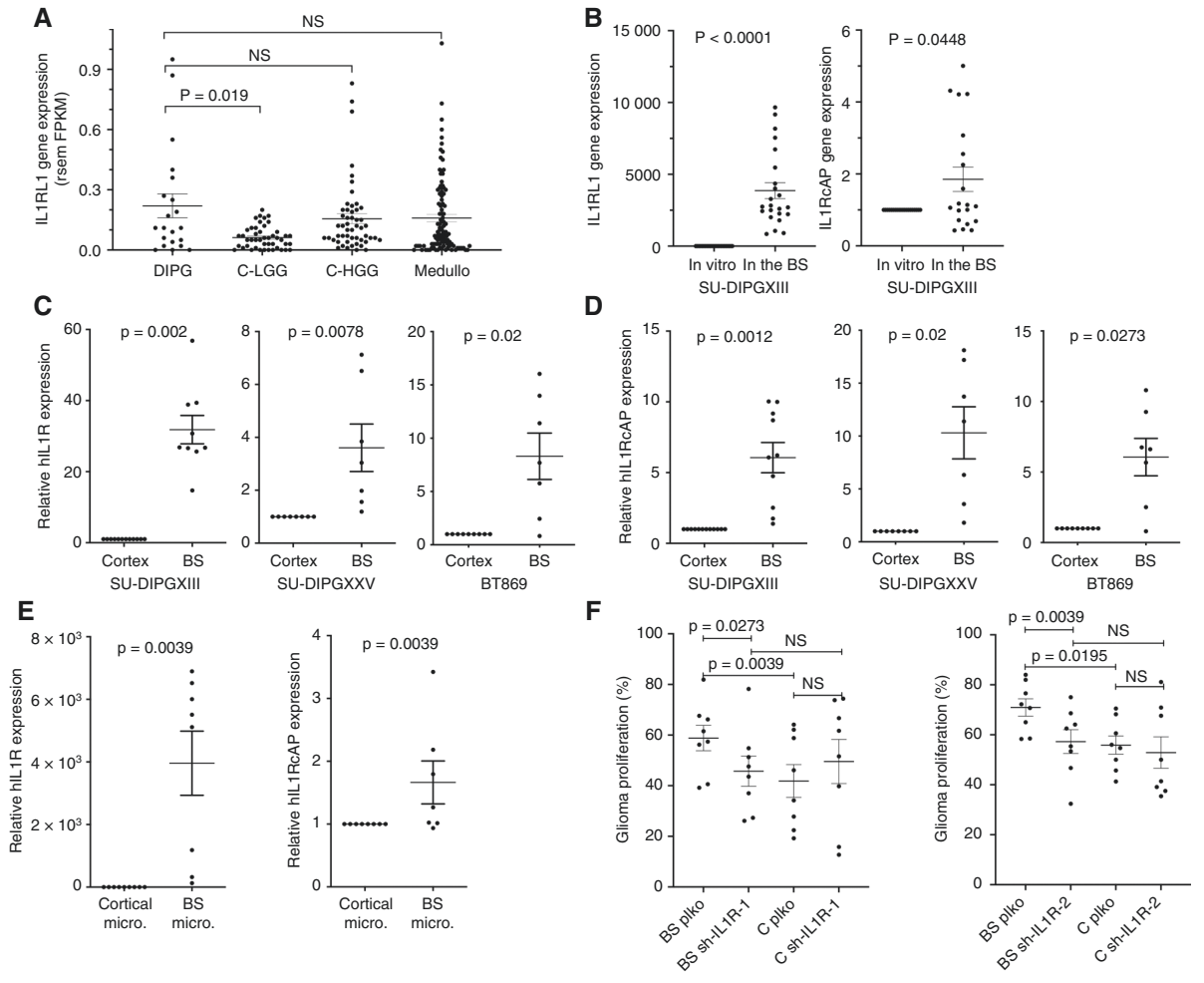

Figure 5. IL33's receptors are involved in glioma–brainstem crosstalk. (a) Human IL1RL1 gene expression data obtained from PedcBioPortal. The gene's expression within biopsies from DIPG samples was compared to cortical low- and high-grade gliomas and to medulloblastoma biopsies. Each point on the graph represents a single human sample, FPKM = fragments per kilobase of exon per million mapped fragments, RSEM = RNA-Seq by Expectation-Maximization (Mann–Whitney *U* test was performed). (b) qPCR analysis of IL1RL1 and IL1RAcP expression in SU-DIPGXIII cells, cultured for 72 h or injected into mouse brainstems and incubated for 72 h (Wilcoxon's signed-rank test, one tailed; IL1RL1 $n = 24$ and IL1RcAP $n = 20$). (c, d) qPCR analysis of IL1RL1 (c) and IL1RcAP (d) expression in glioma cells which were injected into the brainstem or cortex of mice, and then incubated in slice culture for 72 h (Wilcoxon's signed-rank test, one tailed; SU-DIPGXIII $n = 9$, SU- DIPGXXV $n = 8$, BT869 $n = 9$). (e) qPCR analysis of IL1RL1 and IL1RcAP expression in SU-DIPGXIII cells incubated for 72 h on purified microglia cultures from either the brainstem or the cortex (Wilcoxon's signed-rank test, one tailed; IL1RL1 $n = 9$ and IL1RcAP $n = 8$). **For all qPCR analyses, the values are expressed as the average fold change in the brainstems in comparison to the corresponding cortexes ± SEM. (f) IL1RL1 knockdown's effect on SU-DIPGXIII proliferation in ex vivo slice culture. Flow cytometry analysis of CellTrace dye staining of GFP + SU-DIPGXIII cells which underwent IL1RL1 knockdown using two separate shRNAs, 72-h postinjection into the cortex and brainstem of the same brain. For each brain, a parallel injection of control (plko) shRNA-treated cells was performed on the other side. Each point on the graph represents the percentage of GFP + cells which underwent division (at least 1), out of the entire GFP + cell population ± SEM (Wilcoxon's signed-rank test, one tailed; sh-IL1R-1, sh-IL1R-2 $n = 8$).

Our findings support the idea that at a young age, the microenvironment of the brainstem is better able to foster the progression of DIPG tumor cells. Interestingly, these differential effects were in most cases specific to DIPGs as compared to pediatric cortical HGG lines, suggesting a cell-intrinsic component of the tumor cells.

The pro-tumor activity of microglia and macrophages is well documented in adult gliomas.[23] As in other gliomas, microglia/macrophages account for a significant portion of the cellular mass of DIPGs.[33] Although the involvement of microglia in promoting DIPG propagation may not be surprising in itself, the differential ability of brainstem microglia as compared to cortical microglia to promote DIPG growth is striking. In recent years, there has been accumulating evidence indicating differences in microglial populations throughout different brain regions including anatomical cell number distribution, cell density and morphology, molecular signature, and functional differences.[6,34–38] Here we show that microglia differentially support cancer cells based on their anatomical location, partly via IL33.

Accumulating evidence suggests a role for IL33 in adult glioma. Higher expression of IL33 in human glioma specimens has been reported[26,27] and is associated with poor prognosis.[28,32] IL33 has been shown to act directly on glioma cell migration, invasion, and growth.[26–28,31] The role of IL33 in pediatric HGGs has not previously been explored. Based on our findings here and on published data, IL33 is more highly expressed in the brainstem and particularly in the pons of young mice as compared to the cortex (from P2 to P23).[39] According to the Allen Brain Atlas, by day 56, there are no longer any spatial differences in IL33 expression in mice.[40] Also, IL33 is more highly expressed in childhood DIPG biopsies, possibly indicating similar expression patterns in humans and a tumorigenic role. Furthermore, IL1RL1's expression in DIPGs is upregulated in brainstem slices, and specifically by brainstem microglia, while inhibiting IL33 and IL1RL1 decreases DIPG proliferation in an anatomically specific manner. All of this suggesting a signaling system that is modulated by the native tumor surroundings. Together, the expression data and the effect on DIPGs proliferation, colony formation, and 3D growth, in culture as well as in brainstem slices, make IL33 a likely factor in the brainstem's microenvironment that contributes to the affinity of DIPGs to this location. However, since the impact of IL33 inhibition on animal survival was not tested here, future testing using in vivo mouse models will be needed before considering reagents such as IL33-blocking antibody ANB020, as a possible therapy in DIPG cases.

Supplementary material

Supplementary material is available online at *Neuro-Oncology Advances* online.

Keywords

DIPG | interleukin-33 | pediatric high-grade gliomas | microglia

Funding

This work was supported by a grant from the Israel Cancer Research Fund [grant number 01948, OB]; the Israeli Ministry of Health [grant number 3011003086, OB]; Israel Cancer Association [grant number 20210011, OB]; and by a generous support from the Pakula family (OB). This work was also supported by Dana-Farber Pediatric Low Grade Astrocytoma Foundation (RS); Koch Institute Bridge Program grant (DAL); NCI PSON [grant number U54-CA210180 (DAL); and NIH [grant number U01-CA215798 (DAL)].

Acknowledgments

We thank the Koch Institute's Robert A. Swanson (1969) Biotechnology Center for technical support, specifically the Bioinformatics Facility. We also thank the Hebrew University, Faculty of Medicine Core Research Facility, and particularly to Zakhariya Manevitch for valuable help with the two-photon microscopy. We thank Keith L. Ligon (Dana-Farber Cancer Institute) for BT869, and Michelle Monje (Stanford University School of Medicine) for the SU-pcGBM2, SU-DIPGXXV, and SU-DIPGXIII. We are grateful to Dr. Norman Grover (Department of Experimental Medicine, The Hebrew University) for helpful advice regarding the statistical analyses.

Conflict of interest statement. The authors declare no potential conflicts of interest.

Authorship

L.P.Z conducted all experiments and contributed to experimental design, manuscript editing, and data analysis for all sections. L.A and N.C contributed to conducting in vitro experiments. V.B and S.B.C contributed to conducting ex vivo experiments. D.A.L, S-H.B.K, and M.J.L RNA contributed to experimental design and performed the RNA-seq bioinformatics analysis. R.U. and O.A. preformed the human tumor bioinformatics analysis. M.G.F and R.S. contributed to experimental design and manuscript editing. O.B. designed all experiments, wrote the manuscript, and supervised all aspects of the work.

References

1. Cosnarovici MM, Cosnarovici RV, Piciu D. Updates on the 2016 World Health Organization Classification of Pediatric Tumors of the Central Nervous System – a systematic review. *Med Pharmacy Rep.* 2021;94(3):282–288.
2. Mackay A, Burford A, Carvalho D, et al. Integrated molecular meta-analysis of 1,000 pediatric high-grade and diffuse intrinsic pontine glioma. *Cancer Cell* 2017;32(4):520–537.e5.
3. Juratli TA, Qin N, Cahill DP, Filbin MG. Molecular pathogenesis and therapeutic implications in pediatric high-grade gliomas. *Pharmacol Ther.* 2018;182:70–79. doi:10.1016/j.pharmthera.2017.08.006
4. Schwartzentruber J, Korshunov A, Liu X-Y, et al. Driver mutations in histone H3.3 and chromatin remodelling genes in paediatric glioblastoma. *Nature* 2012;482(7384):226–231.
5. Pathania M, De Jay N, Maestro N, et al. H3.3K27M cooperates with Trp53 loss and PDGFRA gain in mouse embryonic neural progenitor cells to induce invasive high-grade gliomas. *Cancer Cell* 2017;32(5):684–700.e9.
6. Grabert K, Michoel T, Karavolos MH, et al. Microglial brain region-dependent diversity and selective regional sensitivities to aging. *Nat Neurosci.* 2016;19(3):504–516.
7. Marques S, Zeisel A, Codeluppi S, et al. Oligodendrocyte heterogeneity in the mouse juvenile and adult central nervous system. *Science* 2016;352(6291):1326–1329.
8. Molofsky AV, Kelley KW, Tsai H-H, et al. Astrocyte-encoded positional cues maintain sensorimotor circuit integrity. *Nature* 2014;509(7499):189–194.

9. Morel L, Chiang MSR, Higashimori H, et al. Molecular and functional properties of regional astrocytes in the adult brain. *J Neurosci.* 2017;37(36):8706–8717.
10. Tsai H-H, Li H, Fuentealba LC, et al. Regional astrocyte allocation regulates CNS synaptogenesis and repair. *Science* 2012;337(6092):358–362.
11. Charles NA, Holland EC, Gilbertson R, Glass R, Kettenmann H. The brain tumor microenvironment. *Glia* 2011;59(8):1169–1180.
12. Pyonteck SM, Akkari L, Schuhmacher AJ, et al. CSF-1R inhibition alters macrophage polarization and blocks glioma progression. *Nat Med.* 2013;19(10):1264–1272.
13. Silver DJ, Siebzehnrubl FA, Schildts MJ, et al. Chondroitin sulfate proteoglycans potently inhibit invasion and serve as a central organizer of the brain tumor microenvironment. *J Neurosci.* 2013;33(39):15603–15617.
14. Venkatesh HS, Johung TB, Caretti V, et al. Neuronal activity promotes glioma growth through neuroligin-3 secretion. *Cell* 2015;161(4):803–816.
15. Venkatesh HS, Tam LT, Woo PJ, et al. Targeting neuronal activity-regulated neuroligin-3 dependency in high-grade glioma. *Nature* 2017;549(7673):533–537.
16. Ben-Gigi L, Sweetat S, Besser E, et al. Astrogliosis induced by brain injury is regulated by sema4b phosphorylation. *eNeuro* 2015;2(3):ENEURO.0078–ENEU14.2015.
17. Bronstein R, Torres L, Nissen JC, Tsirka SE. Culturing microglia from the neonatal and adult central nervous system. *J Vis Exp.* 2013(78):50647. doi:10.3791/50647
18. Alcoser SY, Kimmel DJ, Borgel SD, et al. Real-time PCR-based assay to quantify the relative amount of human and mouse tissue present in tumor xenografts. *BMC Biotechnol.* 2011;11:124. doi:10.1186/1472-6750-11-124
19. Cerami E, Gao J, Dogrusoz U, et al. The cBio cancer genomics portal: an open platform for exploring multidimensional cancer genomics data. *Cancer Discov.* 2012;2(5):401–404.
20. Gao J, Aksoy BA, Dogrusoz U, et al. Integrative analysis of complex cancer genomics and clinical profiles using the cBioPortal. *Sci Signal.* 2013;6(269):pl1.
21. Peretz L, Besser E, Hajbi R, et al. Combined shRNA over CRISPR/cas9 as a methodology to detect off-target effects and a potential compensatory mechanism. *Sci Rep.* 2018;8(1):93.
22. Gutmann DH, Kettenmann H. Microglia/brain macrophages as central drivers of brain tumor pathobiology. *Neuron* 2019;104(3):442–449.
23. Hambardzumyan D, Gutmann DH, Kettenmann H. The role of microglia and macrophages in glioma maintenance and progression. *Nat Neurosci.* 2016;19(1):20–27.
24. Keane L, Cheray M, Saidi D, et al. Inhibition of microglial EZH2 leads to anti-tumoral effects in pediatric diffuse midline gliomas. *Neurooncol Adv.* 2021;3(1):vdab096.
25. Ross JL, Chen Z, Herting CJ, et al. Platelet-derived growth factor beta is a potent inflammatory driver in paediatric high-grade glioma. *Brain* 2021;144(1):53–69.
26. De Boeck A, Ahn BY, D'Mello C, et al. Glioma-derived IL-33 orchestrates an inflammatory brain tumor microenvironment that accelerates glioma progression. *Nat Commun.* 2020;11(1):4997.
27. Zhang J-F, Wang P, Yan Y-J, et al. IL-33 enhances glioma cell migration and invasion by upregulation of MMP2 and MMP9 via the ST2-NF-κB pathway. *Oncol Rep.* 2017;38(4):2033–2042.
28. Zhang J, Wang P, Ji W, Ding Y, Lu X. Overexpression of interleukin-33 is associated with poor prognosis of patients with glioma. *Int J Neurosci.* 2017;127(3):210–217.
29. Taniguchi S, Elhance A, Van Duzer A, et al. Tumor-initiating cells establish an IL-33-TGF-β niche signaling loop to promote cancer progression. *Science* 2020;369(6501–6513):eaay1813.
30. Li Y, Shi J, Qi S, et al. IL-33 facilitates proliferation of colorectal cancer dependent on COX2/PGE2. *J Exp Clin Cancer Res.* 2018;37(1):196.
31. Zhang J-F, Tao T, Wang K, et al. IL-33/ST2 axis promotes glioblastoma cell invasion by accumulating tenascin-C. *Sci Rep.* 2019;9(1):20276.
32. Gramatzki D, Frei K, Cathomas G, et al. Interleukin-33 in human gliomas: expression and prognostic significance. *Oncol Lett.* 2016;12(1):445–452.
33. Caretti V, Sewing ACP, Lagerweij T, et al. Human pontine glioma cells can induce murine tumors. *Acta Neuropathol.* 2014;127(6):897–909.
34. Tan Y-L, Yuan Y, Tian L. Microglial regional heterogeneity and its role in the brain. *Mol Psychiatry* 2020;25(2):351–367.
35. Hammond TR, Dufort C, Dissing-Olesen L, et al. Single-cell RNA sequencing of microglia throughout the mouse lifespan and in the injured brain reveals complex cell-state changes. *Immunity* 2019;50(1):253–271.e6.
36. De Biase LM, Schuebel KE, Fusfeld ZH, et al. Local cues establish and maintain region-specific phenotypes of basal ganglia microglia. *Neuron* 2017;95(2):341–356.e6.
37. Marshall GP, Deleyrolle LP, Reynolds BA, Steindler DA, Laywell ED. Microglia from neurogenic and non-neurogenic regions display differential proliferative potential and neuroblast support. *Front Cell Neurosci.* 2014;8:180.
38. O'Koren EG, Yu C, Klingeborn M, et al. Microglial function is distinct in different anatomical locations during retinal homeostasis and degeneration. *Immunity* 2019;50(3):723–737.e7.
39. Wicher G, Husic E, Nilsson G, Forsberg-Nilsson K. Developmental expression of IL-33 in the mouse brain. *Neurosci Lett.* 2013;555:171–176. doi:10.1016/j.neulet.2013.09.046
40. Lein ES, Hawrylycz MJ, Ao N, et al. Genome-wide atlas of gene expression in the adult mouse brain. *Nature* 2007;445(7124):168–176.